



Influence of Mn substitution on crystal structure and magnetic properties of $Y_2Zr_{1-x}Ti_{1-x}Mn_{2x}O_7$ ($x = 0.0, 0.05, 0.10$) family of pyrochlore oxides

Mukesh Kumar Verma¹ · Devinder Singh¹

Received: 14 July 2020 / Revised: 7 November 2020 / Accepted: 18 November 2020 / Published online: 23 November 2020
© Australian Ceramic Society 2020

Abstract

The present paper deals with the effect of Mn doping on structural and magnetic properties of $Y_2Zr_{1-x}Ti_{1-x}Mn_{2x}O_7$ ($x = 0.0, 0.05, 0.10$) compounds. All the samples are single phase and crystallize in the cubic system with $Fd-3m$ space group. Both lattice parameter a and cell volume V decrease with Mn substitution because of the smaller ionic radius of Mn^{4+} than Zr^{4+} and Ti^{4+} . No significant differences between zero field-cooled (ZFC) and field-cooled (FC) curves are evident, demonstrating that the samples exhibit no magnetic ordering or spin glass-like transition. Both the Mn-doped phases exhibit antiferromagnetic behavior, which may possibly be due to the presence of super-exchange (SE) $Mn^{4+}-O^{2-}-Mn^{4+}$ interactions. Small magnetic hysteresis loops are observed for the Mn-doped phases suggesting the presence of weak ferromagnetic interactions.

Keywords Pyrochlores · Pechini method · XRD · Magnetic properties

Introduction

Pyrochlore oxides of the type $A_2B_2O_7$ have been of great interest for many researchers over a number of years due to their fascinating properties and potential advantages. These materials have great photocatalytic activity, exotic magnetic properties, multiferroic behavior, dielectric tunability, order/disorder transformations, and a range of electrical and ionic conductivities that include semiconducting, metallic, and superconductivity. Because of these properties, they are utilized as fast ion conductors, magnetic materials, and thermal barrier coating materials in gas turbines [1–7]. Moreover, their unusual chemical stability and flexibility to form solid solutions with several cations make them suitable as a host matrix for immobilizing radiotoxic nuclear waste [8, 9].

Pyrochlore oxides of formula $A_2B_2O_7$ have a cubic structure, crystallizing in $Fd-3m$ space group, with all atoms occupying specific locations. A is usually a trivalent rare-earth ion located at the $16c$ site but can also be a mono- or divalent cation, and B may be a 3d, 4d, or 5d transition element located at the $16d$ site having a suitable oxidation state for charge

balance with the stoichiometry $A_2B_2O_7$ [10, 11]. Three sites ($48f$, $8a$, $8b$) are free for oxygen in this structure. In the perfectly ordered pyrochlore structure, O atoms are present at $8a$ and $48f$ sites leaving the $8b$ site vacant. There is only one variable positional parameter x which represents the position of the O atoms on the $48f$ site (x , $1/8$, $1/8$). The coordination number of larger A site cation is 8 while that of smaller B cation is 6 forming BO_6 octahedra. Of the seven O atoms, one is separate from the BO_6 octahedra, and its only bond is to the A cation, positioned in the voids between BO_6 octahedra. Hence, the crystal structure can be seen as a network of distorted BO_6 octahedra that share vertices with angles B–O–B close to 130° , making a system of interconnected tunnels that can be regarded as the backbone of the structure.

One intriguing characteristic of pyrochlore-type materials is the structural transformation from their ordered form to a disordered defect fluorite structure with changes in either of the stoichiometry, temperature, or pressure [12, 13]. The pyrochlore structure is nearly correlated to defect fluorite structure. The unit cell parameters of pyrochlore are double to that of defect fluorite. Not all compounds with stoichiometry $A_2B_2O_7$ form the pyrochlore cubic structure. The structural stability of pyrochlore is usually associated to the ratio of the ionic radii of the A and B type cations (r_A/r_B) lying within the limit 1.29–2.30 [12]. Radius ratio less than 1.29 is expected to exhibit the fluorite structure. It should be remarked that the

✉ Devinder Singh
drdssambyal@rediffmail.com

¹ Department of Chemistry, University of Jammu, Jammu, India

numerical value of the radius ratio (r_A/r_B) is adopted only as a widespread guideline in view of some exceptions [14].

Pyrochlores comprising the 2nd and 3rd row transition metals have recently attracted noteworthy interest due to their exceptional magneto-transport properties. The pyrochlore lattice containing Zr at the B site is thought to be the potent host matrix for fixation of nuclear wastes as it can hold significant quantities of actinides and lanthanides in its structure [15]. $Gd_2Zr_2O_7$ is a well-investigated pyrochlore, which is one of the most encouraging materials but with comparatively low thermal conductivity. Pyrochlore-structured $Sm_2Zr_2O_7$ is reported to have good conducting properties relative to other low-temperature ionic conductors [16]. Geometrically frustrated Ti-containing pyrochlores of composition $Ln_2Ti_2O_7$ have been widely investigated due to their novel characteristics such as spin ice behavior in $Dy_2Ti_2O_7$ and $Ho_2Ti_2O_7$ [17, 18] and spin liquid state in $Tb_2Ti_2O_7$ [19]. Most of the Ti-containing rare-earth pyrochlore oxides show antiferromagnetic interactions. Doping of Zr in the site of Ti in $Gd_2(Ti_{1-x}Zr_x)_2O_7$ system results in a two-order rise in the ionic conductivity which is associated to an increase in the anion disorder [11]. Kumar et al. have explored the magnetic properties of pyrochlore oxides with both Zr and Ti at the B site [20]. As the doping of other cations at the A and B site takes place which changes the radius ratio, more disorder between the cation sites can arise resulting in the transformation of the pyrochlore phase and a change in properties. Pyrochlores with Mn at the B site exhibit fascinating magnetic properties [21–24]. Liang et al. reported that in the $Bi_2Ir_{2-x}Mn_xO_7$ system antiferromagnetic (AFM) interactions are increased at the start with increase in Mn content, which are then reduced with further increase in Mn content [25].

As far as we know, there are limited reports in literature where Mn is substituted for Zr and Ti at the B site. In view of this, we have synthesized pyrochlore oxides with composition $Y_2Zr_{1-x}Ti_{1-x}Mn_{2x}O_7$ ($x = 0.0, 0.05, 0.10$) via the sol-gel Pechini method which needs neither high heating temperature nor long calcination times and hence is advantageous over the solid-state reaction method. The present work aims to study the effect of substitution of larger Zr and Ti ions by smaller Mn ion which shift the structure toward more ordered pyrochlore form. Moreover, the effect on magnetic properties with different doping levels of Mn has also been explored.

Experimental

In the present work, $Y_2Zr_{1-x}Ti_{1-x}Mn_{2x}O_7$ ($x = 0.0, 0.05, 0.10$) powders were prepared via Pechini method using Y_2O_3 (Loba Chemicals), $ZrO(NO_3)_2 \cdot H_2O$ (Alfa Aesar), $C_{12}H_{28}O_4Ti$ (Alfa Aesar), $Mn(CH_3COO)_2 \cdot 4H_2O$ (Loba Chemicals), citric acid monohydrate (Loba Chemicals), and polyethylene glycol (Loba Chemicals) as preliminary materials. Analytical grade

(99.9% purity) chemical reagents were used in the present study. The stoichiometric amounts of Y_2O_3 , $ZrO(NO_3)_2 \cdot H_2O$, and $Mn(CH_3COO)_2 \cdot 4H_2O$ were dissolved in minimum volume of 3 N HNO_3 with consistent stirring at 80 °C to convert them into metal nitrates. The extra nitric acid was dissipated by heating the resulting nitrate solution on a hot plate followed by the addition of deionized water to these metal nitrates with constant stirring for 30 min. The stoichiometric amount of liquid $C_{12}H_{28}O_4Ti$ was then added to the solution and stirred using a magnetic stirrer until a clear solution is formed. An appropriate amount of citric acid (CA) in the molar ratio of citric acid/metal cations as 3:1 was then added to get the metal citrate solution followed by the addition of polyethylene glycol in the molar ratio of 4:1 with citric acid. The resulting solution was then stirred for 30 min. To evaporate the excess solvents and to promote polymerization, the solution was kept on a hot plate at 80 °C ending in a yellow clear viscous solution succeeded by the appearance of the gel. The gel was then decomposed in an oven at 200 °C resulting in a foamy and voluminous combustion residue. The fluffy mass was readily crushed into the precursor powder and transferred into silica crucible which was then thermally treated at 500 °C in a muffle furnace to decompose the organic precursor. After grinding, the powders were pressed into pellets under pressure and then calcined in air at 1250 °C for 24 h with two intermittent grindings to get pure crystalline samples.

Elucidation of crystal structure was done by powder X-ray diffraction (PANanalytical X'Pert PROMRD, the Netherlands, using Ni-filtered CuK_{α} radiations) at room temperature with 2θ varied in the range of 10–100°. Scanning electron microscopy (FE-SEM QUANTA 200 FEG from FEI, the Netherlands, with accelerating voltage 0.3–30 kV) was used to analyze the surface morphology and microstructures. The compositional purity and stoichiometry of various cations were checked by energy-dispersive X-ray spectroscopy (EDX) using INCA attachment with the SEM instrument. Temperature-dependent magnetization measurements in the range 10–300 K in both ZFC and FC conditions and field-dependent magnetization measurements with an applied field of $-70 \text{ kOe} < H < 70 \text{ kOe}$ were conducted by means of Quantum Design MPMS-3 SQUID magnetometer.

Results and discussion

Structural characterization

Purity and the crystal structure of $Y_2Zr_{1-x}Ti_{1-x}Mn_{2x}O_7$ ($x = 0.0, 0.05, 0.10$) were checked by powder XRD. Figure 1 shows the XRD patterns of the three $Y_2Zr_{1-x}Ti_{1-x}Mn_{2x}O_7$ compounds. The sharp and intense peaks within the diffraction pattern coinciding with the pyrochlore structure were seen, implying good crystalline forms for samples. All the

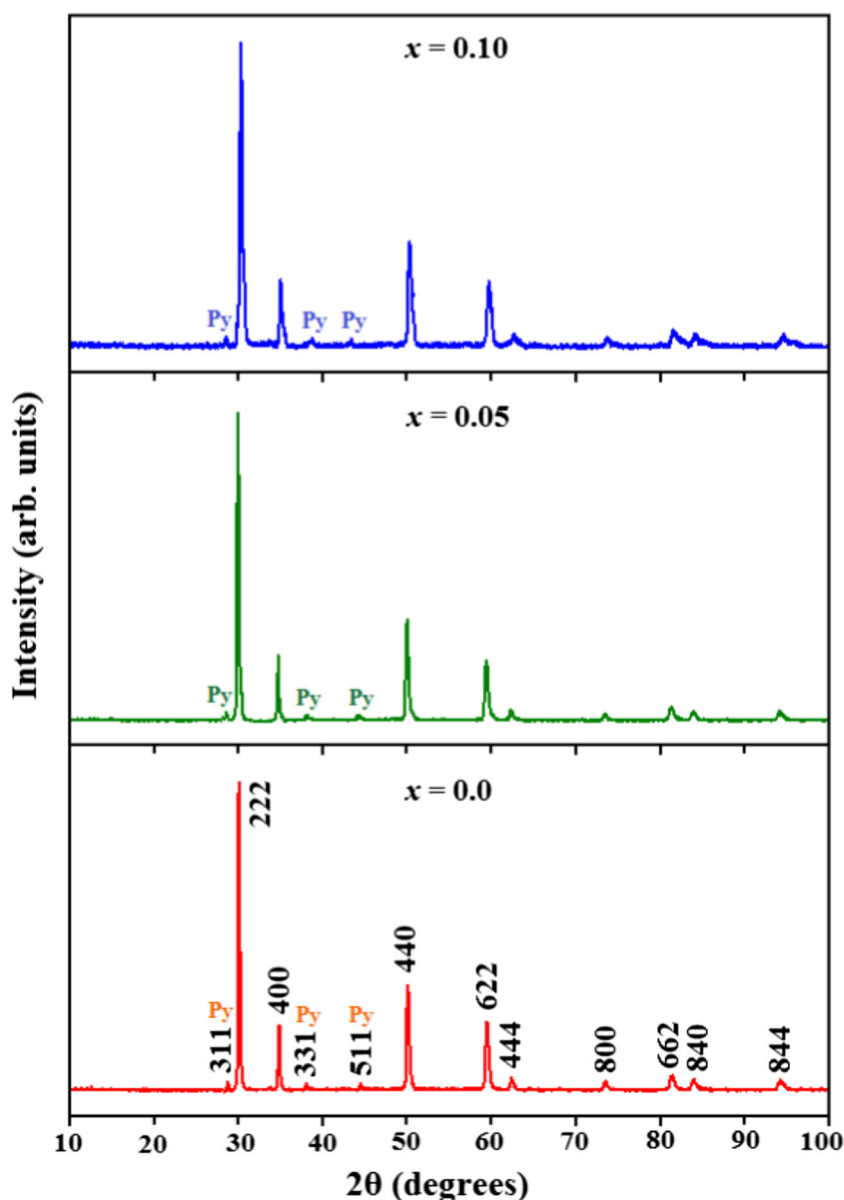
Table 1 Lattice parameter (*a*), unit cell volume (*V*), and crystallite size (*D*) obtained from X-ray diffraction data for $Y_2Zr_{1-x}Ti_{1-x}Mn_{2x}O_7$

Composition	<i>x</i> = 0.0	<i>x</i> = 0.05	<i>x</i> = 0.10
<i>a</i> (Å)	10.2818(1)	10.2617(2)	10.2555(1)
<i>V</i> (Å ³)	1086.94(2)	1080.58(4)	1078.62(2)
<i>D</i> (nm)	92.3	92.1	91.6

peaks can be well indexed by the pyrochlore structure in cubic system with space group *Fd-3m* [25–28] and matched well with standard pattern (JCPDS 16-0400). The diffraction pattern of pyrochlore is basically that of the fluorite structure along with a set of low-intensity diffraction peaks at about the 2θ values of 14° (111), 28° (311), 37° (331), 45° (511),

and 51° (531), which correspond to the ordering in the lattice. It may be noted that reflections (111) and (531) were not observed in the present case. These missing reflections have also been reported by a number of researchers [25, 27, 29]. The superstructure peaks of the ordered lattice are specified by a Py label in the Fig. 1. There is no evidence to suggest the precipitation of any secondary phase from the solid solutions indicated by absence of impurity peaks in the diffraction pattern. The lattice parameter *a* and unit cell volume *V* are given in Table 1. It has been noted that both the lattice parameter *a* and cell volume *V* decrease with increase in *x* because of the substitution of larger Zr^{4+} and Ti^{4+} with smaller Mn^{4+} ion. Moreover, from the values of ratio of the average A site radius to the average B site radius (r_A/r_B), it has been observed that with the substitution of a smaller Mn^{4+} ion into the Zr^{4+} and

Fig. 1 Typical Miller-indexed XRD patterns for $Y_2Zr_{1-x}Ti_{1-x}Mn_{2x}O_7$



Ti⁴⁺ site, the value of r_A/r_B increases, resulting in the ordering of pyrochlore structure.

The average crystallite size (D) was calculated by applying the Scherrer equation, given below, to the most intense XRD peak (222) as a reference plane [30],

$$D = \frac{K\lambda}{\beta \cos\theta}$$

where K is the shape factor (=0.90), λ is the X-ray wavelength, θ corresponds to the peak position, and β is full width at half maximum of (222) peak in radians. The results (Table 1) show no appreciable difference in crystallite size for the samples. This might be due to formation of stable pyrochlore structure for all the $Y_2Zr_{1-x}Ti_{1-x}Mn_{2x}O_7$ ($x = 0.0, 0.05, 0.10$) samples.

Elemental and microstructural analysis

To check the elemental composition of the phases, EDX analyses are conducted (Fig. 2). It gives the qualitative elemental composition in the samples by the appearance of Y, Zr, Ti, and Mn metal peaks. The results (mass percentage of elements present) confirmed the existence of the constitutive elements and did not show any impurity element in the phases. The mass percentages calculated from the EDX data are found near to the nominal compositions as presented in Table 2.

Analysis of surface morphology and microstructures of the prepared phases was done by SEM. The SEM profile of phases is displayed in Fig. 3. All the samples show more or less alike near spherical morphology. The average grain size calculated from SEM images using line intercept method falls in the submicron range. Agglomeration of particles with high homogeneity has also been observed to a certain extent.

Magnetic properties

A systematic study of temperature-dependent magnetic susceptibility for all samples has been accomplished using both ZFC and FC modes at very low applied magnetic field (100 Oe) as shown in the Fig. 4. It can be seen that there is no change in magnetic susceptibility for the parent sample

Table 2 EDX results of the $Y_2Zr_{1-x}Ti_{1-x}Mn_{2x}O_7$

Compound	$x = 0.0$		$x = 0.05$		$x = 0.10$	
	Mass%		Mass%		Mass%	
	Exp.	Cal.	Exp.	Cal.	Exp.	Cal.
Y	41.54	41.46	41.69	41.60	41.70	41.74
Zr	21.19	21.27	20.22	20.27	19.38	19.27
Ti	11.27	11.16	10.76	10.64	10.15	10.11
Mn			1.24	1.28	2.63	2.58

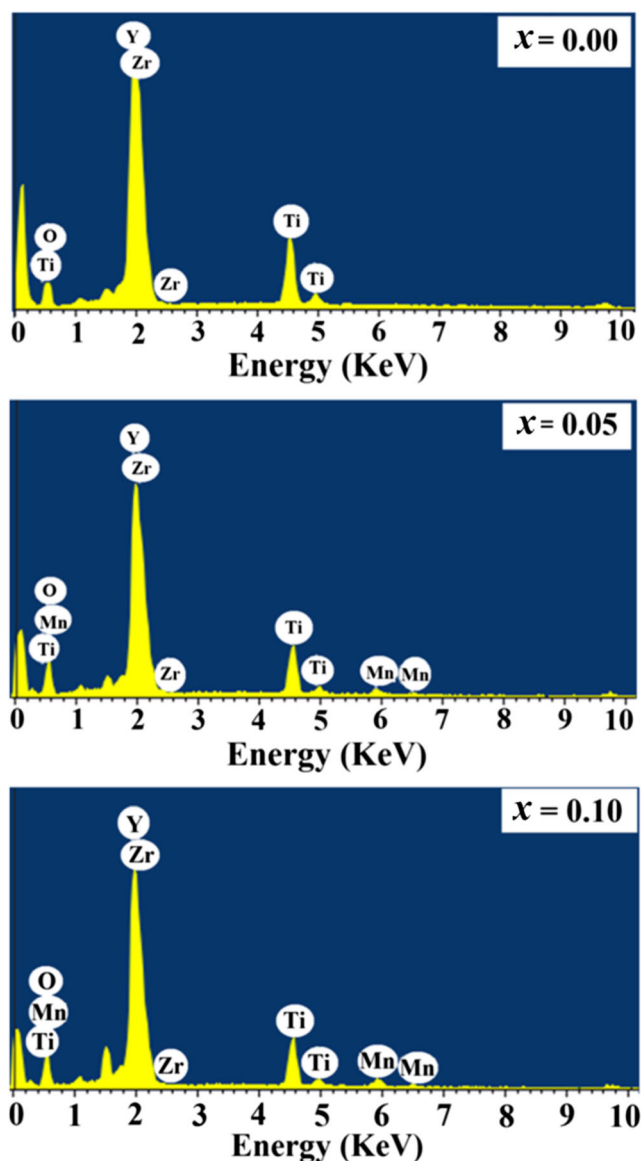


Fig. 2 EDX spectra of $Y_2Zr_{1-x}Ti_{1-x}Mn_{2x}O_7$

with $x = 0.0$, which could obviously be due to the fact that all the ions in the sample are diamagnetic in character. Moreover, in the case of Mn-doped samples, no significant differences between ZFC and FC curves are evident. This shows that the samples obeyed the canonical paramagnetic behavior, with no magnetic ordering or spin glass-like transition. Similar behavior was also observed for rare-earth-doped Ti pyrochlores [31].

The thermal variation of the reciprocal ZFC molar magnetic susceptibility for Mn doped samples is displayed in Fig. 5. The linear part of inverse molar magnetic susceptibility data at high temperature (170–300 K) for $x = 0.10$ sample was fitted using the Curie-Weiss law [32],

$$\chi_m = \frac{C}{T - \Theta}$$

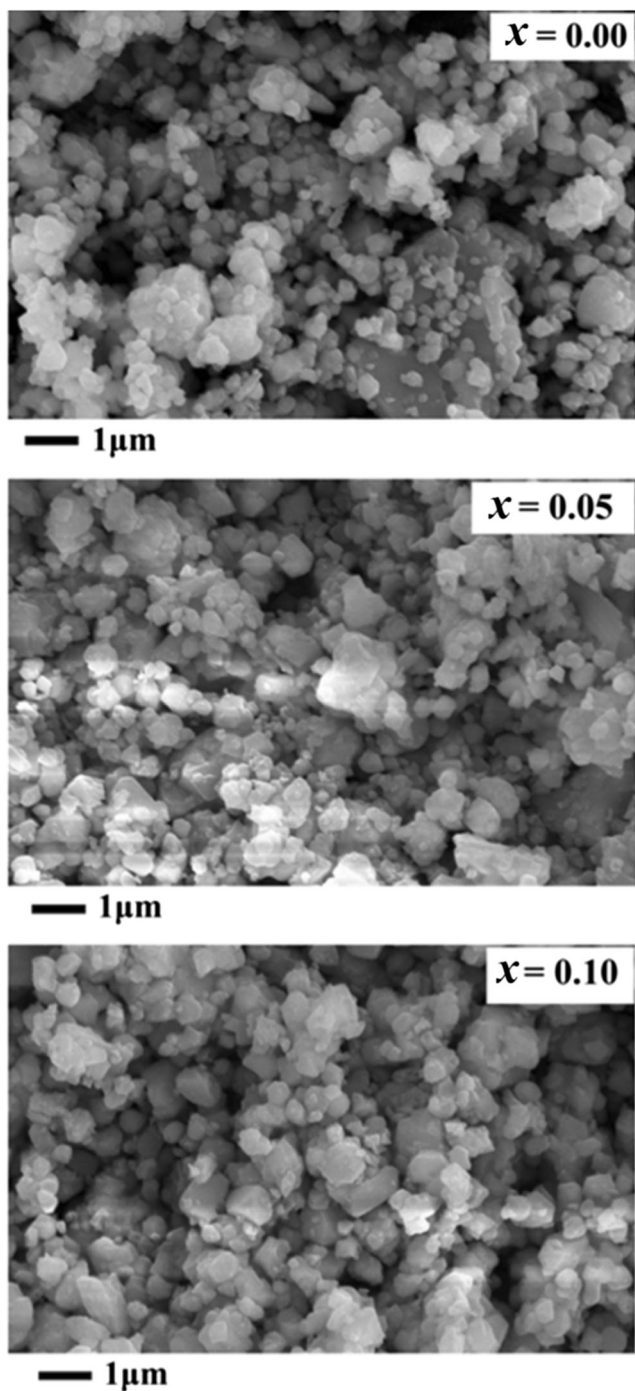


Fig. 3 SEM micrographs of $Y_2Zr_{1-x}Ti_{1-x}Mn_{2x}O_7$

where C is the Curie constant and Θ is the Curie-Weiss temperature, while $x = 0.05$ sample does not show any linearity in the investigated temperature range.

The effective magnetic moment (μ_{eff}) of $x = 0.10$ phase in the temperature range of implementation of the Curie-Weiss law was calculated from the Curie constant (derived from the slope of $\chi_m^{-1} - T$ plot) by the following relation:

$$\mu_{eff} = 2.828\sqrt{C}$$

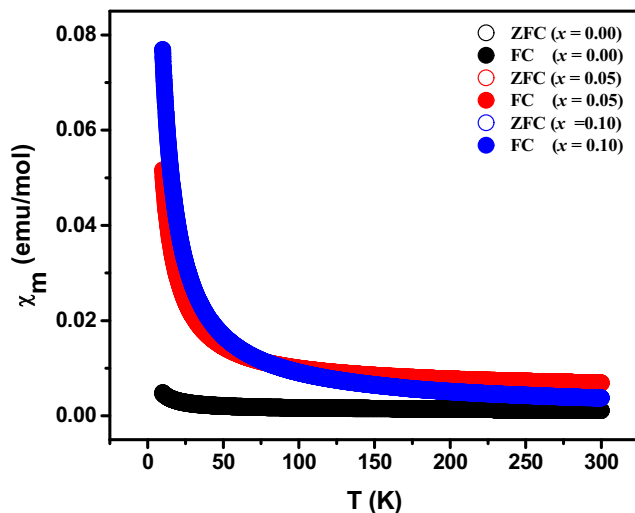


Fig. 4 Temperature dependence of molar magnetic susceptibility (χ_m) for $Y_2Zr_{1-x}Ti_{1-x}Mn_{2x}O_7$

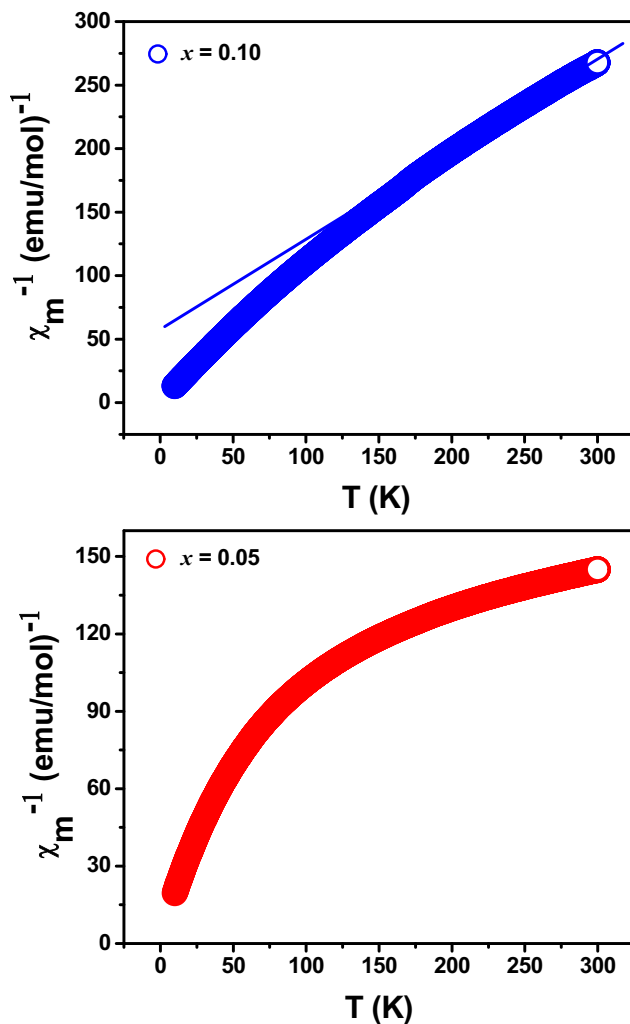


Fig. 5 Plots of temperature dependent inverse molar magnetic susceptibility (χ_m^{-1}) for the $Y_2Zr_{1-x}Ti_{1-x}Mn_{2x}O_7$

Table 3 Magnetic parameters of $Y_2Zr_{1-x}Ti_{1-x}Mn_{2x}O_7$

Compound	Θ (K)	μ_{eff} (B.M.)	μ_{cal} (B.M.)	M_s (emu/g)	μ_s (B.M.)	$\mu_{s(\text{th})}$ (B.M.)	$\Delta\mu = \mu_{s(\text{th})} - \mu_s$
$x = 0.05$	–	–	–	3.36	0.26	0.3	0.04
$x = 0.10$	– 80	2.07	1.73	5.05	0.38	0.6	0.22

We have also calculated the value of theoretical magnetic moment (μ_{cal}) of $x = 0.10$ phase by the relationship [33, 34],

$$\mu_{\text{cal}} = \sqrt{x\mu_{Mn^{4+}}^2}$$

where x is the fraction of Mn^{4+} ions in the samples and $\mu_{Mn^{4+}}$ (3.87 B.M.) is its spin only magnetic moment. The values of Θ , μ_{eff} , and μ_{cal} for $x = 0.10$ sample are listed in Table 3. The negative value of Θ shows that antiferromagnetic interactions are dominant in the phase. The antiferromagnetic (AFM) behavior in the material might be due to the presence of super-exchange $Mn^{4+}-O^{2-}-Mn^{4+}$ interactions.

To obtain more extensive information of the magnetic properties, magnetization (M) versus applied magnetic field ($-70 \text{ kOe} < H < 70 \text{ kOe}$) measurements at 10 K has been made for both Mn-doped samples. The $M-H$ curves for the samples are shown in Fig. 6. Furthermore, magnetic hysteresis loops are perceived for the Mn-doped compositions implying that the systems have dominant antiferromagnetic (AFM) interactions with a weak ferromagnetic component. The extent of unsaturation in the $M-H$ curves becomes progressively more marked with increase in Mn concentration, which might be due to increase in super-exchange $Mn^{4+}-O^{2-}-Mn^{4+}$ interactions. Further, it is thought that the presence of weak ferromagnetic component in the phases is due to the canted antiferromagnetic arrangement instead of ferromagnetic order. The magnetization

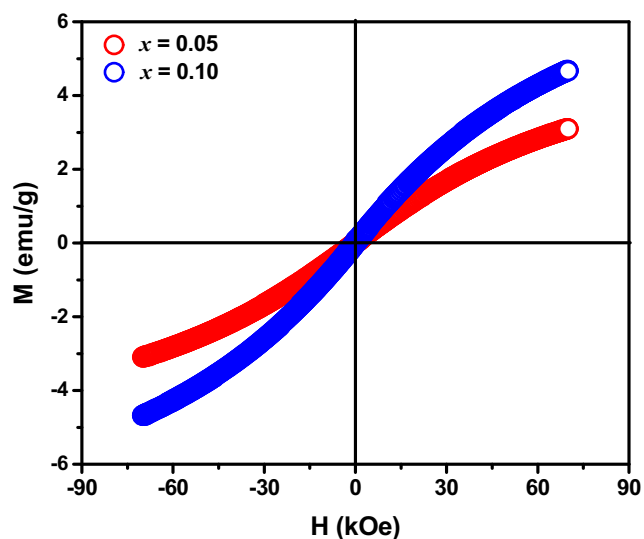


Fig. 6 Variation of magnetization (M) as a function of magnetic field (H) for $Y_2Zr_{1-x}Ti_{1-x}Mn_{2x}O_7$

does not saturate even at the maximum applied field of 70 kOe for both Mn-doped phases. Then, the saturation magnetization (M_s) was determined from the plot between M and $1/H$ in the high field zone. The values of saturation magnetization are monotonically increasing with Mn doping level (Table 3). Using the hysteresis curve shown in Fig. 6, it is possible to estimate the magnitude of the uncompensated moment (μ_s) per formula unit from M_s , the values of which are given in Table 3. These values are found to be smaller than theoretical value $\mu_{s(\text{th})}$ (Table 3) corresponding to high-spin state for Mn^{4+} and ferromagnetic (FM) ordering of all spins which proves that the dominating magnetic behavior is AFM, which is consistent with present data of negative Curie-Weiss temperature (Θ). Further, the increase in the value of $\Delta\mu$ with Mn doping indicates the presence of greater AFM interactions as a result of increase in super-exchange $Mn^{4+}-O^{2-}-Mn^{4+}$ interactions.

Conclusion

In summary, we have studied the structural and magnetic properties of $Y_2Zr_{1-x}Ti_{1-x}Mn_{2x}O_7$ ($x = 0, 0.05, 0.10$) compounds synthesized by Pechini method. All the phases crystallize in the cubic system with $Fd-3m$ space group. The decrease in lattice parameter a and cell volume V with Mn doping is attributed to smaller ionic radius of Mn^{4+} than Zr^{4+} and Ti^{4+} . No magnetic ordering or spin glass-like transition was observed at low temperature. The negative value of Θ suggests that AFM interactions are dominant in the Mn-doped phases. Moreover, small magnetic hysteresis loops are observed for the Mn-doped phases suggesting the presence of weak ferromagnetic interactions.

Compliance with ethical standards

Conflict of interest The authors declare that they have no conflict of interest.

References

- Chamberlain, S.L., Hess, S., Corruccini, L.R.: Dipolar magnetic order in the pyrochlore structure. *Phys. Lett. A.* **323**, 310–314 (2004)
- Raju, N.P., Dion, M., Gingras, M.J.P., Mason, T.E., Greedan, J.E.: Transition to long-range magnetic order in the highly frustrated

- insulating pyrochlore antiferromagnet $\text{Gd}_2\text{Ti}_2\text{O}_7$. *Phys. Rev. B.* **59**, 14489–14498 (1999)
3. Lian, J., Wang, L.M., Wang, S.X., Chen, J., Boatner, L.A., Ewing, R.C.: Nanoscale manipulation of pyrochlore: new nanocomposite ionic conductors. *Phys. Rev. Lett.* **87**(1–4), 145901 (2001)
 4. Poulsen, F.W., Glerup, M., Holtappels, P.: Structure, Raman spectra and defect chemistry modelling of conductive pyrochlore oxides. *Solid State Ionics.* **135**, 595–602 (2000)
 5. Wilde, P.J., Catlow, C.R.: Molecular dynamics study of the effect of doping and disorder on diffusion in gadolinium zirconate. *Solid State Ionics.* **112**, 185–195 (1998)
 6. Dong, X.W., Wang, K.F., Luo, S.J., Wan, J.G., Liu, J.M.: Coexistence of magnetic and ferroelectric behaviors of pyrochlore $\text{Ho}_2\text{Ti}_2\text{O}_7$. *J. Appl. Phys.* **106**(1–4), 104101 (2009)
 7. Mirsaneh, M., Hayden, B.E., Furman, E., Perini, S., Lanagan, M.T., Reaney, I.M.: High dielectric tunability in lead niobate pyrochlore films. *Appl. Phys. Lett.* **100**(1–3), 082901 (2012)
 8. Wang, S.X., Wang, L.M., Ewing, R.C., Kutty, K.G.: Ion irradiation of rare-earth and yttrium-titanate-pyrochlores. *Nucl. Instr. Meth. Phys. Res. B.* **169**, 135–140 (2000)
 9. Reid, D.P., Stennett, M.C., Hyatt, N.C.: The fluorite related modulated structures of the $\text{Gd}_2(\text{Zr}_{2-x}\text{Ce}_x)\text{O}_7$ solid solution: an analogue for Pu disposition. *J. Solid State Chem.* **191**, 2–9 (2012)
 10. Chen, Z.S., Gong, W.P., Chen, T.F., Li, S.L.: Synthesis and characterization of pyrochlore-type yttrium titanate nanoparticles by modified sol-gel method. *Bull. Mater. Sci.* **34**, 429–434 (2011)
 11. Moon, P.K., Tuller, H.L.: Ionic conduction in the $\text{Gd}_2\text{Ti}_2\text{O}_7$ – $\text{Gd}_2\text{Zr}_2\text{O}_7$ system. *Solid State Ionics.* **28**, 470–474 (1988)
 12. Subramanian, M.A., Aravamudan, G., Rao, G.S.: Oxide pyrochlores—a review. *Prog. Solid State Chem.* **15**, 55–143 (1983)
 13. Wang, J., Nakamura, A., Takeda, M.: Structural properties of the fluorite and pyrochlore-type compounds in the Gd_2O_3 – ZrO_2 system $x\text{GdO}_{1.5}$ – $(1-x)\text{ZrO}_2$ with $0.18 \leq x \leq 0.62$. *Solid State Ionics.* **164**, 185–191 (2003)
 14. Mandal, B.P., Garg, N., Sharma, S.M., Tyagi, A.K.: Preparation, XRD and Raman spectroscopic studies on new compounds $\text{RE}_2\text{Hf}_2\text{O}_7$ (RE = Dy, Ho, Er, Tm, Lu, Y): pyrochlores or defect-fluorite? *J. Solid State Chem.* **179**, 1990–1994 (2006)
 15. Muromura, T., Hinatsu, Y.: Fluorite type phase in nuclear waste ceramics with high zirconia and alumina contents. *J. Nucl. Mater.* **151**, 55–62 (1987)
 16. Shinozaki, K., Miyauchi, M., Kuroda, K., Sakurai, O., Mizutani, N., Kato, M.: Oxygen-ion conduction in the $\text{Sm}_2\text{Zr}_2\text{O}_7$ pyrochlore phase. *J. Am. Ceram. Soc.* **62**, 538–539 (1979)
 17. Harris, M.J., Bramwell, S.T., McMorrow, D.F., Zeiske, T.H., Godfrey, K.W.: Geometrical frustration in the ferromagnetic pyrochlore $\text{Ho}_2\text{Ti}_2\text{O}_7$. *Phys. Rev. Lett.* **79**, 2554–2557 (1997)
 18. Ramirez, A.P., Hayashi, A., Cava, R.J., Siddharthan, R., Shastry, B.S.: Zero-point entropy in ‘spin ice’. *Nature.* **399**, 333–335 (1999)
 19. Gingras, M.J., Den Hertog, B.C., Faucher, M., Gardner, J.S., Dunsiger, S.R., Chang, L.J., Gaulin, B.D., Raju, N.P., Greedan, J.E.: Thermodynamic and single-ion properties of Tb^{3+} within the collective paramagnetic-spin liquid state of the frustrated pyrochlore antiferromagnet $\text{Tb}_2\text{Ti}_2\text{O}_7$. *Phys. Rev. B.* **62**, 6496–6511 (2000)
 20. Kumar, B.V., Velchuri, R., Devi, V.R., Sreedhar, B., Prasad, G., Prakash, D.J., Kanagaraj, M., Arumugam, S., Vithal, M.: Preparation, characterization, magnetic susceptibility (Eu, Gd and Sm) and XPS studies of $\text{Ln}_2\text{ZrTiO}_7$ (Ln = La, Eu, Dy and Gd). *J. Solid State Chem.* **184**, 264–272 (2011)
 21. Kennedy, B.J., Hunter, B.A.: Structural and magnetic studies of manganese-containing pyrochlore oxides. *J. Alloys Compd.* **302**, 94–100 (2000)
 22. Reimers, J.N., Greedan, J.E., Kremer, R.K., Gmelin, E., Subramanian, M.A.: Short-range magnetic ordering in the highly frustrated pyrochlore $\text{Y}_2\text{Mn}_2\text{O}_7$. *Phys. Rev. B.* **43**, 3387–3394 (1991)
 23. Raju, N.P., Greedan, J.E., Subramanian, M.A.: Magnetic, electrical, and small-angle neutron-scattering studies of possible long-range order in the pyrochlores $\text{Tl}_2\text{Mn}_2\text{O}_7$ and $\text{In}_2\text{Mn}_2\text{O}_7$. *Phys. Rev. B.* **49**, 1086–1091 (1994)
 24. Shimakawa, Y., Kubo, Y., Manako, T.: Giant magnetoresistance in $\text{Ti}_2\text{Mn}_2\text{O}_7$ with the pyrochlore structure. *Nature.* **379**, 53–55 (1996)
 25. Liang, D., Liu, H., Ling, L., Zhang, L., Zhang, C., Zhang, Y.: Magnetic and magnetoelectric properties of hybrid-frustrated $\text{Bi}_2\text{Ir}_{2-x}\text{Mn}_x\text{O}_7$ pyrochlores. *Solid State Commun.* **278**, 36–41 (2018)
 26. Liang, D., Liu, H., Liu, N., Ling, L., Han, Y., Zhang, L., Zhang, C.: Structural, magnetic and electrical properties in the pyrochlore oxide $\text{Bi}_{2-x}\text{Ca}_x\text{Ir}_2\text{O}_{7-\delta}$. *Ceram. Int.* **42**, 4562–4566 (2016)
 27. Feng, Y., Zhu, S., Bian, J., Chen, F., Chen, S., Ma, C., Liu, H., Fang, B.: Magnetic and electrical transport properties of the pyrochlore iridate $\text{Bi}_{2-x}\text{Co}_x\text{Ir}_2\text{O}_7$. *J. Magn. Magn. Mater.* **451**, 283–287 (2018)
 28. Karamat, N., Ali, I., Aziz, A., Sher, M., Ashiq, M.N.: Electrical and dielectric studies of substituted holmium based pyrochlore zirconates nanomaterials. *J. Alloys Compd.* **652**, 83–90 (2015)
 29. Zhang, A., Lu, M., Yang, Z., Zhou, G., Zhou, Y.: Systematic research on $\text{RE}_2\text{Zr}_2\text{O}_7$ (RE = La, Nd, Eu and Y) nanocrystals: preparation, structure and photoluminescence characterization. *Solid State Sci.* **10**, 74–81 (2008)
 30. Klug, H.P., Alexander, L.E.: X-ray diffraction procedures; for polycrystalline and amorphous materials. John Wiley and Sons Inc, New York (1954)
 31. Gómez-Pérez, A., Prado-Gonjal, J., Muñoz-Gil, D., Andrada-Chacón, A., Sánchez-Benítez, J., Morán, E., Azcondo, M.T., Amador, U., Schmidt, R.: Anti-site disorder and physical properties in microwave synthesized $\text{RE}_2\text{Ti}_2\text{O}_7$ (RE = Gd, Ho) pyrochlores. *RSC Adv.* **5**, 85229–85241 (2015)
 32. Kittel, C., McEuen, P.: Introduction to solid state physics, pp. 404–406. Wiley, New York (1986)
 33. Singh, D., Mahajan, A.: Effect of A-site cation size on the structural, magnetic, and electrical properties of $\text{La}_{1-x}\text{Nd}_x\text{Mn}_{0.5}\text{Cr}_{0.5}\text{O}_3$ perovskites. *J. Alloys Compd.* **644**, 172–179 (2015)
 34. Sharma, N.D., Sharma, S., Choudhary, N., Verma, M.K., Singh, D.: Comparative study of $\text{La}_{0.5}\text{Nd}_{0.2}\text{Ca}_{0.3-x}\text{K}_x\text{MnO}_3$ ($x = 0.0$ and 0.05) nanoparticles: Effect of A-cation size and calcination temperature. *Ceram. Int.* **45**, 13637–13646 (2019)

Publisher's note Springer Nature remains neutral with regard to jurisdictional claims in published maps and institutional affiliations.